

ARTICLE

DOI: 10.1038/s41467-018-04471-7

OPEN

Tuning the interplay between nematicity and spin fluctuations in $\text{Na}_{1-x}\text{Li}_x\text{FeAs}$ superconductors

S.-H. Baek¹, Dilip Bhoi², Woohyun Nam², Bumsung Lee², D.V. Efremov¹, B. Büchner^{1,3} & Kee Hoon Kim^{2,4}

Strong interplay of spin and charge/orbital degrees of freedom is the fundamental characteristic of the iron-based superconductors (FeSCs), which leads to the emergence of a nematic state as a rule in the vicinity of the antiferromagnetic state. Despite intense debate for many years, however, whether nematicity is driven by spin or orbital fluctuations remains unsettled. Here, by use of transport, magnetization, and ^{75}As nuclear magnetic resonance (NMR) measurements, we show a striking transformation of the relationship between nematicity and spin fluctuations (SFs) in $\text{Na}_{1-x}\text{Li}_x\text{FeAs}$; For $x \leq 0.02$, the nematic transition promotes SFs. In contrast, for $x \geq 0.03$, the system undergoes a non-magnetic phase transition at a temperature T_0 into a distinct nematic state that suppresses SFs. Such a drastic change of the spin fluctuation spectrum associated with nematicity by small doping is highly unusual, and provides insights into the origin and nature of nematicity in FeSCs.

¹IFW Dresden, Helmholtzstr. 20, 01069 Dresden, Germany. ²Department of Physics and Astronomy, Center for Novel State of Complex Materials Research, Seoul National University, Seoul 151-747, Korea. ³Department of Physics, Technische Universität Dresden, 01062 Dresden, Germany. ⁴Department of Physics and Astronomy, Institute of Applied Physics, Seoul National University, Seoul 151-747, Korea. Correspondence and requests for materials should be addressed to S.-H.B. (email: sbaek.fu@gmail.com) or to K.H.K. (email: optopia@snu.ac.kr)

Nematicity, i.e., spontaneous breaking of the C_4 symmetry of the crystal, has emerged as a research focus recently in the iron-based superconductors (FeSCs), because the nematic state can provide a clue to the understanding of high temperature superconductivity in these materials^{1–8}. Currently two major scenarios have been proposed for the origin of nematicity: magnetic and charge/orbital⁹. The former assumes that the nematic state are entirely induced by the interband spin fluctuations (SFs). The latter scenario treats its origin as charge density waves or orbital orders.

The magnetic scenario is believed to be realized in the 122-family of FeSCs^{10–12}, particularly because a scaling relation was found between the spin fluctuations in nuclear magnetic resonance (NMR) and the shear modulus in the tetragonal phase of $\text{Ba}(\text{Fe}_{1-x}\text{Co}_x)_2\text{As}_2$ ¹⁰. On the other hand, the most simple compound FeSe is best described by the orbital scenario since nematic order occurs without any signature of the spin fluctuation enhancement^{13–15}. In FeSCs other than FeSe, however, the SDW transition temperature T_{SDW} is quite close to the nematic one T_{nem} , imposing limitations on investigating the interplay of nematicity and SFs in detail. Thus it is much desirable to find a system in which one can effectively tune SFs and nematicity in wide phase spaces, e.g., temperature and chemical doping.

From this point of view, NaFeAs, which is isostructural and isoelectronic to well investigated LiFeAs, is worth attention. LiFeAs shows only a superconducting (SC) ground state without a signature of nematicity or magnetism^{16–18}. In contrast, NaFeAs is featured by the three successive transitions at low T ; a nematic transition at $T_{\text{nem}} \sim 55$ K is followed by a SDW at $T_{\text{SDW}} \sim 45$ K and by a filamentary SC transition at ~ 8 K. In this respect, the study of (Na,Li)FeAs may allow a full spectrum of emergent orders coming from a delicate balance among competing orders by Li (Na)-substitution into Na (Li) layers in NaFeAs (LiFeAs). However, the study of such isoelectronic doping has been extremely challenging because (Na,Li)FeAs becomes easily phase separated due to distinct chemistry of Na and Li metals.

In this work, we report the successful growth of homogeneous $\text{Na}_{1-x}\text{Li}_x\text{FeAs}$ single crystals and the investigation of their electronic phase diagram up to $x = 0.1$. We found that with a systematic increase of x , the SDW is suppressed for $x \geq 0.03$, giving way to the SC state with the full Meissner shielding. Strikingly, also for $x \geq 0.03$, ⁷⁵As spin-lattice relaxation measurements show a sharp anomaly at a well-defined temperature T_0 , evidencing a non-magnetic phase transition before entering the bulk SC state. Our comprehensive data further show that, above a critical doping $x_c \sim 0.03$, spin and nematic fluctuations become strongly entangled, resulting in a charge/orbital ordered state below T_0 . This implies that the nature of a nematic state could vary depending on the underlying electronic structure. Furthermore, our rich phase diagram strongly suggests that the normal state of FeSCs from which superconductivity emerges is far more complex than previously known.

Results and discussion

Crystal structure. Figure 1a presents the crystal structure and Fig. 1b shows the variation of the c -axis lattice parameter of the $\text{Na}_{1-x}\text{Li}_x\text{FeAs}$ single crystals, which decreases systematically with increasing x up to 0.06 and then levels off from 0.08. The c value was extracted from the (00 l) reflections in the diffraction pattern measured along the ab -plane of the single crystals (Supplementary Fig. 1a) which suggests the absence of any other impurity phase. To determine the crystalline phase, we also performed the powder x -ray diffraction of the ground $\text{Na}_{0.95}\text{Li}_{0.05}\text{FeAs}$ single crystal (Supplementary Fig. 1b) and the pattern could be

successfully refined by the tetragonal $P4/nmm$ structure as in the parent NaFeAs¹⁹.

Transport and magnetization measurements. The temperature (T) dependence of resistivity (ρ) of the selected $\text{Na}_{1-x}\text{Li}_x\text{FeAs}$ single crystals is displayed in the T range from 3 to 300 K, and near the SC transition in Fig. 1d, e, respectively. Each resistivity curve was normalized by the value at 300 K ($\rho/\rho_{300\text{K}}$) and shifted vertically for clarity (for the original resistivity data, see Supplementary Fig. 2). For the undoped crystal, ρ decreases smoothly exhibiting a typical metallic behavior with decreasing T , showing up several anomalous features at low T , an upturn at ~ 54 K (magenta arrow), a first drop (black arrow) at ~ 41 K, and a second drop to reach finally zero resistivity state (blue arrow) at ~ 7.7 K, which are identified as the nematic (T_{nem}), the SDW (T_{SDW}), and the SC (T_c^0) transition temperatures, respectively. T_{nem} and T_{SDW} appear more clearly in the derivative curves of $d\rho/dT$ as a deviation point (magenta arrow in Fig. 1f) and a local maximum or minimum (black arrow in Fig. 1f). At $T_c^0 \sim 7.7$ K, the corresponding magnetic susceptibility (χ) (Fig. 1c) decreases abruptly, allowing us to assign T_c from χ , $T_c^x \sim 7.0$ K. These transport and magnetization data are overall consistent with those found in previous reports on NaFeAs (refs.^{19–24}).

With the same criteria applied on the parent NaFeAs, we could extract the T_c^0 (T_c^x), T_{SDW} , T_{nem} , and Meissner shielding fractions for the whole region ($0 \leq x \leq 0.1$). With increasing doping within $0 \leq x \leq 0.02$, both T_{nem} and T_{SDW} are rapidly suppressed. For $x = 0.03$, the $d\rho/dT$ curve reveals a jump which is assigned to T_{nem} , but does not show an anomaly associated with T_{SDW} . The magnetization data show that the SC volume fraction in the parent compound is very small in agreement with the previous results and increases weakly with doping up to $x \sim 0.03$. Upon further doping ($x = 0.04, 0.05$, and 0.06), the SC shielding fraction at $T = 2$ K reaches 68%, 98%, and 90%, respectively, and the highest $T_c = 12.3$ K is obtained for $x = 0.05$, constituting an optimal doping. After the optimal doping, inserting more dopants into the system suppress both the SC shielding fraction and T_c , and eventually superconductivity disappears above $x = 0.12$.

⁷⁵As nuclear magnetic resonance. We now turn to ⁷⁵As NMR measurements on $\text{Na}_{1-x}\text{Li}_x\text{FeAs}$. The ⁷⁵As nuclei (nuclear spin $I = 3/2$) possess a large quadrupole moment. For axial symmetry, a magnetic field H perpendicular to the principal axis (crystallographic c -axis in our case) yields two satellite lines whose separation is given by the quadrupole frequency ν_Q . Figure 2a shows the ⁷⁵As NMR full spectrum at $H = 9.1$ T parallel to the ab -plane as a function of Li doping in the tetragonal/paramagnetic (PM) phase (at 60 K). Clearly, $\nu_Q = 9.93$ MHz for undoped crystal does not change notably with doping, indicating that the local symmetry or the average electric field gradient (EFG) at the ⁷⁵As is insensitive to Li dopants up to $x = 0.06$. On the other hand, the linewidth of the spectra progressively increases with increasing doping, which is naturally understood by the increase of chemical disorder due to dopants. It should be noted that the relative linewidth of the satellites with respect to the central one, which could be considered as a measure of chemical homogeneity, remains reasonably small up to ~ 10 at $x = 0.06$, in support of the high quality of our samples. Importantly, we do not observe other NMR lines with doping which would have indicated the presence of an impurity phase such as pure LiFeAs. Thus, the evolution of the ⁷⁵As spectra with doping provides local evidence for the successful incorporation of Li dopants into the Na layers of NaFeAs.

In the magnetically ordered state of NaFeAs, the stripe-like arrangement of Fe moments in the ab -plane, by symmetry,

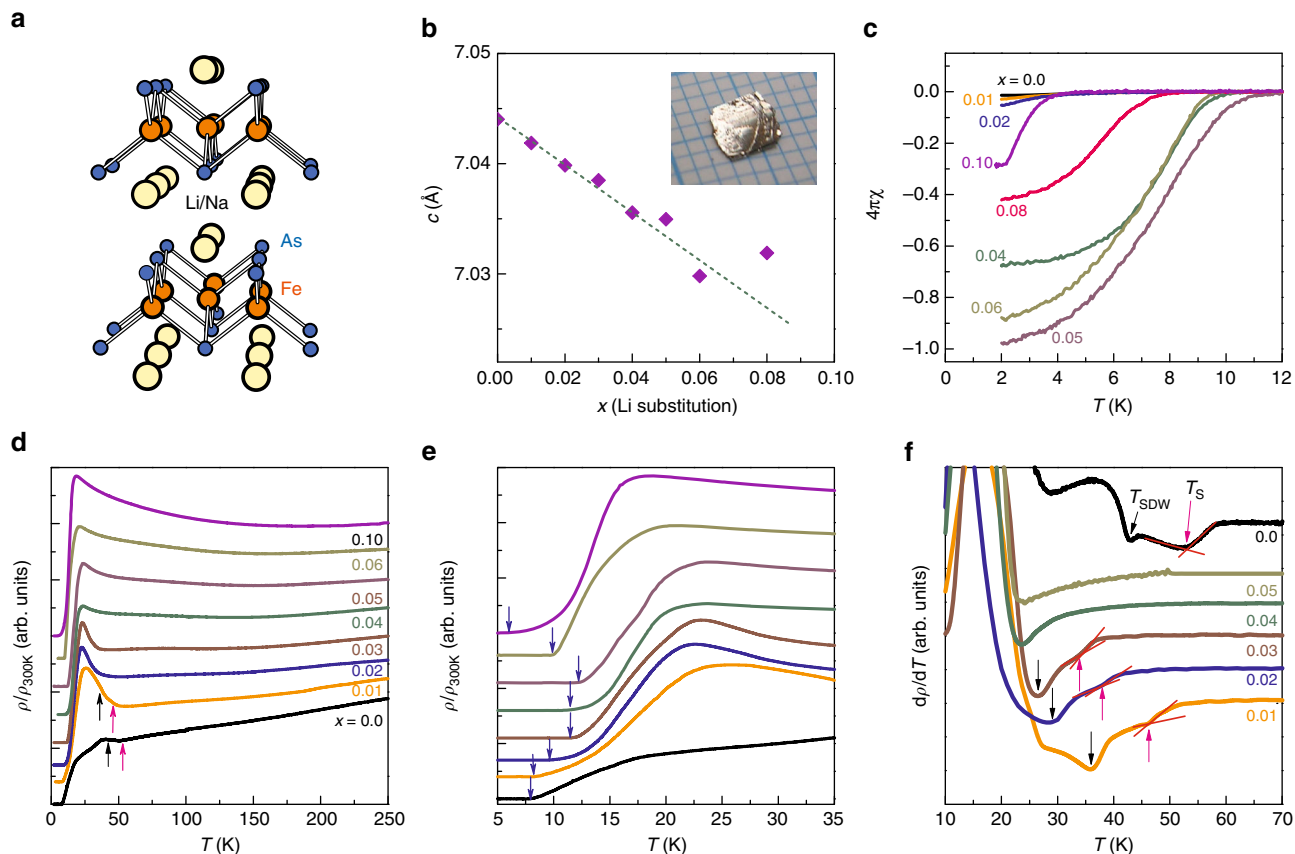


Fig. 1 Characterization of the $\text{Na}_{1-x}\text{Li}_x\text{FeAs}$ single crystals. **a** Crystal structure of $\text{Na}_{1-x}\text{Li}_x\text{FeAs}$. **b** Variation of the c -axis lattice parameter of the $\text{Na}_{1-x}\text{Li}_x\text{FeAs}$ single crystals at 300 K with a linear dashed guide line. Inset shows the ab -plane image of a single crystal in a millimeter scale. **c** Zero-field cooled magnetizations at low temperatures at $H_{ab} = 10$ Oe, revealing SC transition and shielding dependence of normalized resistivity, $\rho/\rho_{300\text{K}}$, enlarged resistivity near the SC transition, and $d\rho/dT$ for selected samples. Black and magenta arrows in **d, f** denote SDW (T_{SDW}) and structural (T_{S}) transitions, respectively, while blue arrows in **e** reflect the T_{c} evolution with x . Note that although previous studies of NaFeAs have observed a local inflection point in the ρ curve at T_{SDW} (or a sharp dip in $d\rho/dT$), we observed weak minimum for our NaFeAs due to the presence of twinning

produces hyperfine fields at ^{75}As pointing along the c -axis^{25, 26}. As a direct consequence of two oppositely aligned antiferromagnetic (AFM) sublattices, the ^{75}As central line splits into two AFM lines for $H \parallel c$. In case of $H \parallel ab$, the total magnetic field that ^{75}As experiences slightly increases due to the vector sum of the local field along c and the external field along ab , and the magnetic broadening of ^{75}As line occurs accordingly. Therefore, long range AFM order in $\text{Na}_{1-x}\text{Li}_x\text{FeAs}$ can be easily confirmed by NMR via a positive shift and a broadening of the ^{75}As line for $H \parallel ab$, and a large AFM splitting of the line for $H \parallel c$. Indeed, for the parent ($x = 0$) and underdoped ($x = 0.02$) samples, the ^{75}As line for $H \parallel ab$ broadens and shifts to higher frequency (Fig. 2b, c), and at the same time the ^{75}As line for $H \parallel c$ splits into two well-defined AFM lines (Fig. 3f), thereby proving locally the SDW order. Note that the splitting of the ^{75}As line shown in Fig. 2b is due to nemacity. Indeed, we determined T_{nem} for $x = 0$ and 0.02 by measuring the T dependence of ^{75}As satellite line (Supplementary Fig. 3).

For $x \geq 0.04$, on the other hand, the T dependence of the ^{75}As spectrum is clearly told apart from those for $x \leq 0.02$ samples. First of all, there is no signature of a static SDW ordering. The ^{75}As line preserves its shape without a shift nor a significant broadening down to low temperatures (see also Supplementary Fig. 4). Second, the T evolution of the ^{75}As spectrum is very similar for the two field orientations $H \parallel ab$ and $H \parallel c$, which contrasts sharply with the strongly anisotropic behavior observed

for $x \leq 0.02$. These features indicate that the system for $x \geq 0.04$ remains paramagnetic. Remarkably, the intermediate doping, i.e., $x = 0.03$, yields a very peculiar feature which seemingly separates the two doping regions, $x \leq 0.02$ and $x \geq 0.04$. That is, the ^{75}As line is considerably broadened below $T_0 \sim 32$ K for both field orientations (see Figs. 2d and 3c). The nearly isotropic NMR line broadening indicates that an inhomogeneous (short-ranged) magnetism develops. Moreover, we emphasize that T_0 for $x = 0.03$ is higher than T_{SDW} for $x = 0.02$ and coincides with T_{nem} (Fig. 4c). Therefore, we conclude that the inhomogeneous line broadening observed for $x = 0.03$ below T_0 is irrelevant to the SDW, but arises from an emerging phase which may involve a short-ranged magnetism.

For $x \geq 0.03$, alongside the suppression of the SDW, we observe that the resonance frequency ν of the ^{75}As line in the PM phase is abruptly reduced. This behavior is clearly shown in Fig. 3g in terms of the Knight shift, $\mathcal{K} \equiv (\nu - \nu_0)/\nu_0 \times 100\%$ where ν_0 is unshifted Larmor frequency. Since the second order quadrupole shift vanishes for $H \parallel c$, $\mathcal{K}_{H \parallel c}$ is equivalent to the local spin susceptibility $\chi_{\text{spin}} = \mu_{\text{B}}^2 N_{\text{F}}$ where N_{F} is the density of states at the Fermi level. While a gradual reduction of χ_{spin} or N_{F} with doping is commonly observed in FeSCs ^{27–29}, the abrupt large reduction of χ_{spin} induced by a moderate doping is very unusual (Supplementary Fig. 5). This may suggest a modification of the Fermi surface geometry near $x \sim 0.03$, owing to, e.g., a Lifshitz transition³⁰.

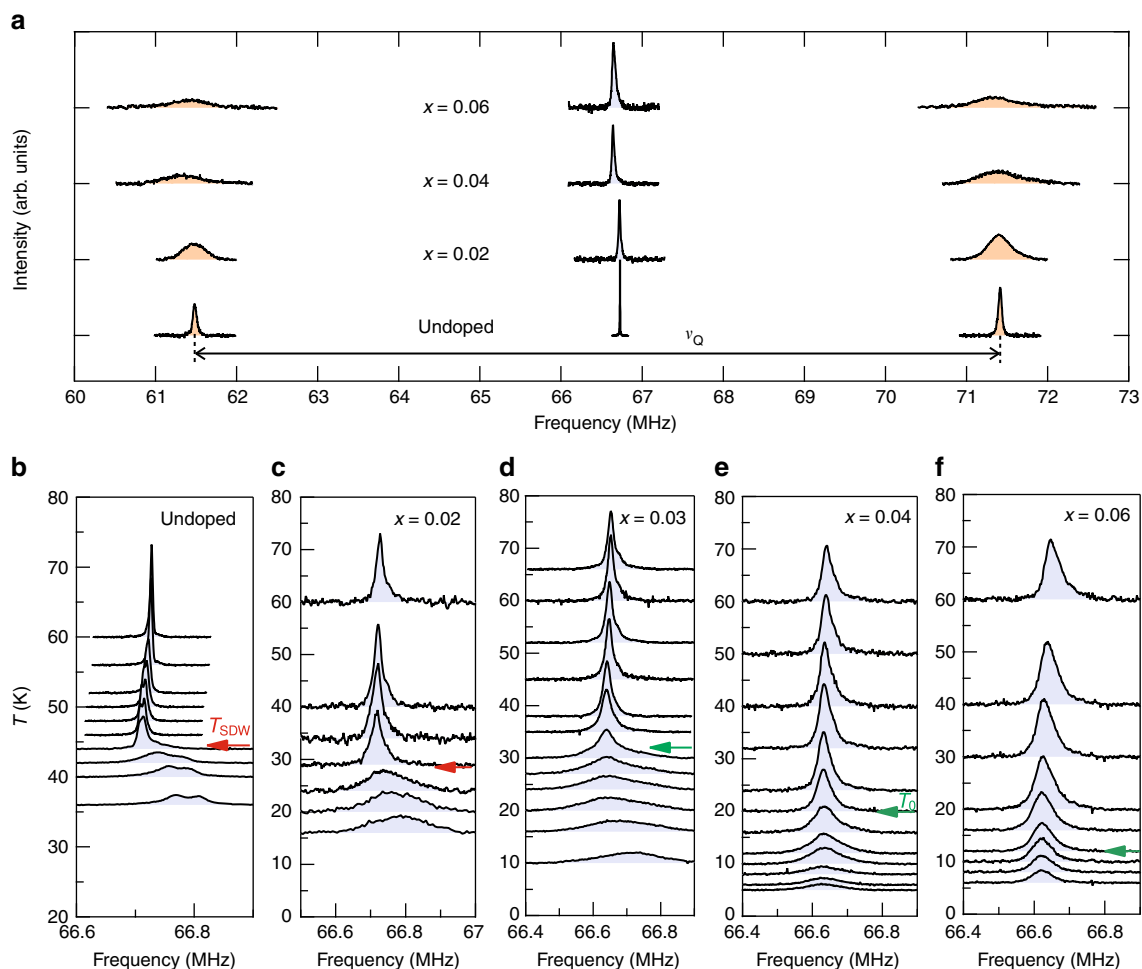


Fig. 2 ^{75}As NMR spectra in $\text{Na}_{1-x}\text{Li}_x\text{FeAs}$ for $H \parallel ab$. **a** Central and satellite lines of ^{75}As as a function of doping at a fixed temperature of 60 K at 9.1 T. While the linewidth of the spectra increases with increasing doping, there is no other lines found and the quadrupole frequency ν_Q remains nearly unchanged. **b-f** Temperature dependence of the ^{75}As central line as a function of x . For $x = 0$ and 0.02, the ^{75}As spectrum starts to broaden and shift to higher frequency below T_{SDW} . In contrast, for $x \geq 0.04$, neither a significant broadening nor a shift of the line was observed, evidencing the absence of static magnetic moments. An inhomogeneous line broadening below T_0 for the intermediate doping $x = 0.03$ is ascribed to short-range magnetism associated with the charge/orbital ordered phase. The large reduction of the signal intensity below ~ 10 K is due to bulk superconductivity

Low energy spin fluctuations. Having established that static SDW order is abruptly suppressed at $x \sim 0.03$, we now investigate low energy spin dynamics, as probed by the spin-lattice relaxation rate divided by temperature $(T_1T)^{-1}$, which is proportional to SFs at very low energy. $(T_1T)^{-1}$ as a function of T and x are shown in Fig. 4. For $x = 0$ and 0.02, the diverging behavior of $(T_1T)^{-1}$ is immediately followed by an exponential drop with decreasing T . The drastic change of $(T_1T)^{-1}$ at T_{SDW} precisely reflects two important characteristics of a SDW transition. The divergence of $(T_1T)^{-1}$ at T_{SDW} represents the critical slowing down of SFs toward long-range magnetic order and the subsequent exponential drop of $(T_1T)^{-1}$ implies the depletion of low-energy spin excitations, i.e., the opening of a SDW gap. As doping is increased to 0.03, the divergent $(T_1T)^{-1}$ observed for $x \leq 0.02$ is greatly suppressed, being consistent with the disappearance of static SDW order for $x \geq 0.03$, as discussed above. Unexpectedly, however, $(T_1T)^{-1}$ drops rapidly below $T_0 > T_c$ forming a peak, indicating a phase transition at T_0 . With further increasing doping, the $(T_1T)^{-1}$ peak gradually moves to lower T , but its shape and height remain nearly the same.

The phase transition at T_0 observed for $x \geq 0.03$ cannot be of magnetic origin. First, the T dependence of the ^{75}As spectrum

(Figs. 2 and 3) does not show any signature of static magnetism, particularly for $x \geq 0.04$. Second, $(T_1T)^{-1}$ or SFs does not diverge at T_0 , implying that the magnetic correlation length remains short at T_0 . Third, the sudden reduction of SFs between $x = 0.02$ and 0.03 is hardly observed in other FeSCs in which SFs above T_{SDW} is gradually suppressed with increasing doping or pressure toward the optimal region^{27, 31, 32}. Moreover, for $x = 0.03$, it turns out that T_0 nearly coincides with T_{nem} , as shown in Fig. 4c, implying that the T_0 transition is closely related to nematicity. Note that the sharp $(T_1T)^{-1}$ peak at T_0 and its doping dependence are well distinguished from those arising from a glassy spin freezing observed in Co-doped BaFe_2As_2 ^{33, 34}; either significant magnetic broadening or strong doping and field dependence of the $(T_1T)^{-1}$ peak expected for a glassy magnetic state is not observed.

Interestingly, we find that the strong anisotropy of $(T_1T)^{-1}$ above T_{SDW} for $x \leq 0.02$ is maintained above T_0 for $x \geq 0.03$ (see Fig. 4a, b). That is, SFs for $H \parallel ab$ is factor of four stronger than for $H \parallel c$ over the whole doping range investigated. The robust spin fluctuation anisotropy with or without a static SDW order indicates that dynamic SDW fluctuations persist at least up to $x = 0.06$.

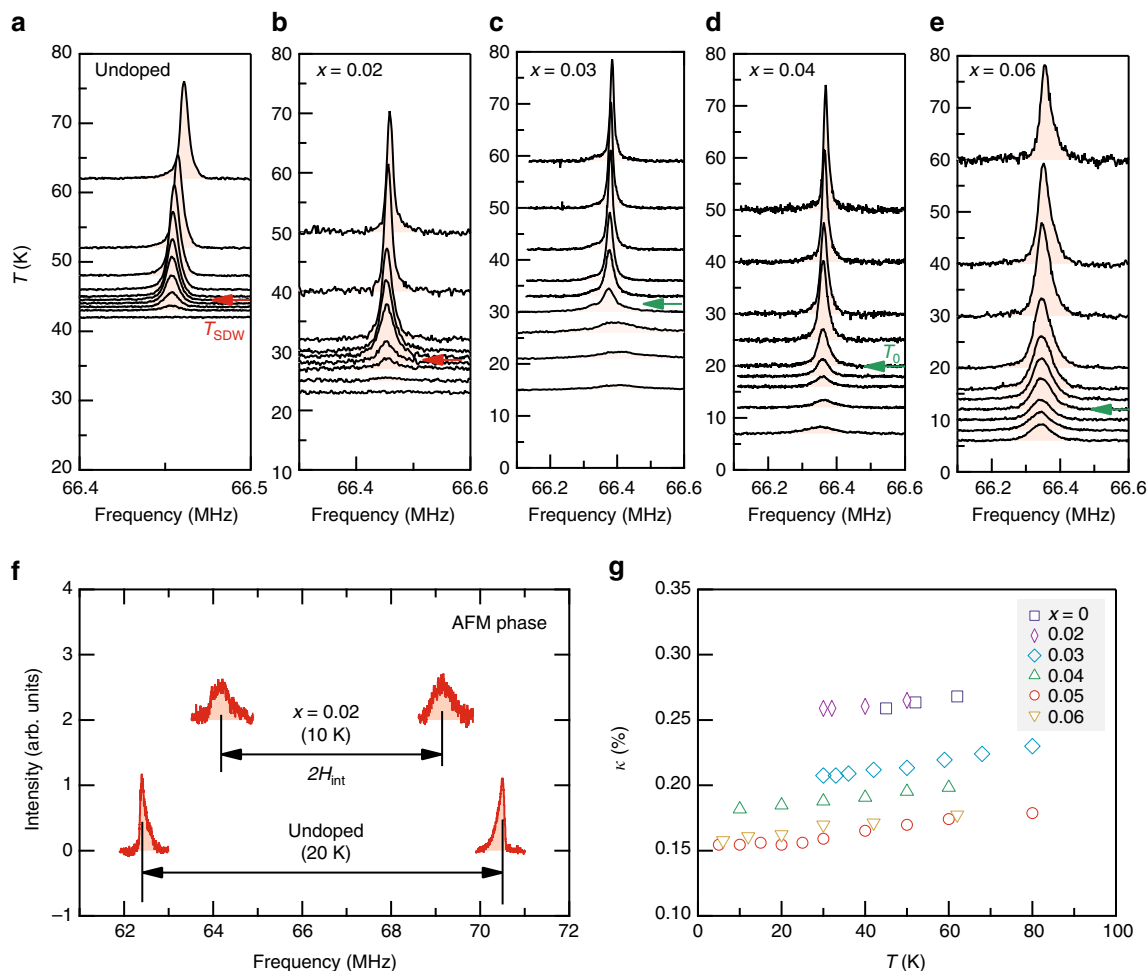


Fig. 3 ^{75}As NMR spectra in $\text{Na}_{1-x}\text{Li}_x\text{FeAs}$ for $H \parallel c$. **a–e** Temperature dependence of the central line as a function of Li doping x measured at 9.1 T. For $x = 0$ and 0.02, the ^{75}As line rapidly disappears below T_{SDW} due to the large hyperfine field resulting from the static Fe spin moment arranged antiferromagnetically. For $x \geq 0.03$, the ^{75}As intensity remains finite down to low temperatures without a significant broadening, indicating the absence of long range magnetic order. **f** The AFM split ^{75}As lines were detected at low temperatures for $x = 0$ and 0.02, manifesting the commensurate AFM phase. **g** The Knight shift \mathcal{K} as a function of temperature and doping at 9.1 T parallel to c . The almost constant \mathcal{K} for a given x is rapidly reduced for $x \geq 0.03$, suggesting a change of the Fermi surface geometry

It may be worthwhile to note that below T_0 the ^{75}As signal amplitude is notably reduced for both $H \parallel ab$ and $H \parallel c$, as shown in Figs. 2d–f and 3c–e (see also Supplementary Fig. 4). The suppression of signal intensity indicates that the volume fraction of the sample seen by NMR decreases in the charge/orbital ordered phase. This phenomenon is quite similar to the wipeout effect observed in the charge stripe phase of cuprate superconductors, in which NMR relaxation rates of the nuclei in spin-rich regions become too fast to be detected^{35–37}. The underlying mechanism of the signal wipeout in $\text{Na}_{1-x}\text{Li}_x\text{FeAs}$ remains unclear and needs further investigation. Interestingly, the similar wipeout of the NMR signal was also observed in the ^{77}Se NMR study of FeSe in the nematic phase which does not involve any static magnetism³⁸.

Phase diagram. Figure 5 presents the temperature-doping phase diagram determined by our NMR and transport/magnetization measurements. When compared to the phase diagram previously known in $\text{NaFe}_{1-x}\text{A}_x\text{As}$ ($A = \text{Co}, \text{Cu}, \text{or Rh}$)^{23, 24, 39, 40}, a difference is the seeming mutual repulsion of the SDW and bulk superconductivity near $x_c \sim 0.03$, similar to that reported in $\text{LaFeAsO}_{1-x}\text{F}_x$ ⁴¹ and $\text{NaFe}_{1-x}\text{Co}_x\text{As}$ ⁴². However, our data are not

sufficiently dense to conclude whether the SDW and SC phases coexist in the narrow doping range near $x = 0.03$ or completely repel each other.

The most important feature in Fig. 5 is the emergence of a non-magnetic phase below $T_0 > T_c$ at optimal doping. Whereas $T_0(x)$ is reasonably connected to T_{nem} for $x \leq 0.02$, we note that the phase below T_0 cannot be a simple nematic because the strong suppression of SFs below T_0 (or spin-gap behavior) is unlikely due to nematicity itself. Although theory predicts that the nematic transition could trigger a pseudogap behavior⁴³, such a pseudogap is only viewed as magnetic precursors whose signature is a sharp increase of the magnetic correlation length. Therefore, we conclude that the phase below T_0 should involve a charge/orbital order which could give rise to a featured gap in the spin fluctuation spectrum.

An even more remarkable observation is the critical change of the relationship between SFs and nematicity with doping. For $x \leq 0.02$, SFs are enhanced just below the nematic transition at T_{nem} and diverge at T_{SDW} . For $x \geq 0.03$, however, a strong enhancement of SFs precedes the phase transition into a charge/orbital nematic state at T_0 , but it is suppressed once the charge/orbital nematic state develops. Theoretically, it has been proposed that

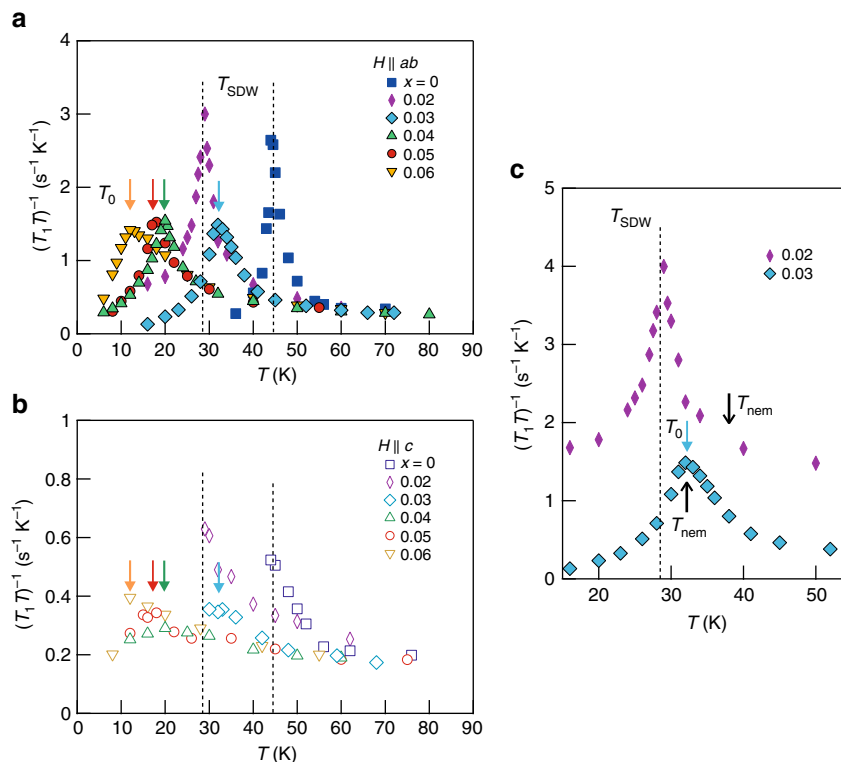


Fig. 4 Spin-lattice relaxation rates as a function of temperature and doping. **a, b** The spin-lattice relaxation rate divided by temperature, $(T_1T)^{-1}$, measured at 9.1 T perpendicular and parallel to c , respectively. For $x = 0$ and 0.02, the SDW transitions were identified by the sharp peak of $(T_1T)^{-1}$ at T_{SDW} . Similar sharp transitions were observed for larger dopings ($x \geq 0.03$) at temperatures denoted by T_0 , without an indication of long range SDW order. The comparison between **a** and **b** reveals that the strong anisotropy of spin fluctuations persists up to $x = 0.06$. **c** Comparison between the $(T_1T)^{-1}$ data for $x = 0.02$ and $x = 0.03$ obtained with $H \parallel ab$. The data for $x = 0.02$ are offset vertically for clarity. It shows that T_0 for $x = 0.03$ is higher than T_{SDW} for $x = 0.02$, but nearly coincides with T_{nem} obtained by resistivity (see Fig. 1)

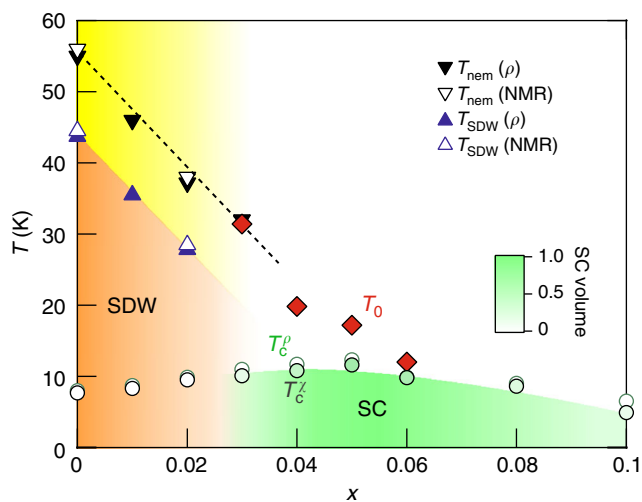


Fig. 5 Temperature-doping phase diagram of $\text{Na}_{1-x}\text{Li}_x\text{FeAs}$. T_{SDW} , T_{nem} , T_c^p , and T_c^s were obtained by our transport, magnetization, and NMR measurements which turn out to be consistent one another. The emerging phase at T_0 before entering the bulk SC state is seemingly connected to the nematic transition at lower dopings. The shade of green below T_c schematically represents the SC volume fraction obtained from Fig. 1c

the strong interplay of spin and charge/orbital degrees of freedom could result in a charge density wave (CDW) state in proximity to a SDW state^{9,44–46}. Following the work⁹, the competition of these two orders can be described by the effective Ginzburg–Landau

functional:

$$\Delta F = \int_{\mathbf{q}} \left(\chi_s^{-1}(\mathbf{q}) (\mathbf{M}_x^2 + \mathbf{M}_y^2) + \chi_c^{-1}(\mathbf{q}) (\Phi_x^2 + \Phi_y^2) \right) + \frac{u}{2} \int_{\mathbf{q}} (\mathbf{M}_x^2 + \mathbf{M}_y^2 + \Phi_x^2 + \Phi_y^2)^2 - \frac{g}{2} \int_{\mathbf{q}} (\mathbf{M}_x^2 - \mathbf{M}_y^2 + \Phi_x^2 - \Phi_y^2)^2, \quad (1)$$

where the $\chi_s(\mathbf{q}, \Omega_n) \sim [\xi_s^{-2} + \alpha_s(q - Q_{x,y})^2]^{-1}$ and $\chi_c(\mathbf{q}, \Omega_n) \sim [\xi_c^{-2} + \alpha_c(q - Q_{x,y})^2]^{-1}$ are dynamical spin and charge susceptibilities, $\mathbf{M}_{x,y}$ and $\Phi_{x,y}$ are SDW and CDW order parameters with the propagation vectors $Q_x = (\pi, 0)$ and $Q_y = (0, \pi)$, respectively. The coupling constant g in the leading order arises due to small non-ellipticity of the electron and hole pockets and is much smaller than u . The onset of nematic order parameter ϕ with $\mathbf{M}_{x,y} = \Phi_{x,y} = 0$ leads to renormalization of the magnetic correlation length $\xi_s^{-2} \rightarrow \xi_s^{-2} \pm \phi$ (see refs.^{9,43}). It leads to strong enhancement of SFs below T_{nem} . The opposite situation happens when the nematic transition coincides with the CDW phase $\Phi_x \neq 0$. The magnetic correlation length changes as $\xi_s^{-2} \rightarrow \xi_s^{-2} + (u \pm g)\Phi_x^2$ leading to suppression of SFs since $(u \pm g) > 0$. This may account for the drastic change of the relationship between nematicity and SFs. Our findings establish $\text{Na}_{1-x}\text{Li}_x\text{FeAs}$ as a rich playground for the study of the interplay of spin and charge/orbital degrees of freedom in FeSCs.

Methods

Crystal growth and characterization. High-quality single crystals of $\text{Na}_{1-x}\text{Li}_x\text{FeAs}$ were grown by a self-flux technique. Due to high reactivity of metallic Na, Li, Fe and As, all preparation processes were carried out inside an Ar-filled glovebox of

which O₂ and H₂O contents were less than 1 ppm. Pure elemental Na (99.995%, Alfa Aesar), Li (99.9 + %, Sigma Aldrich), As (99.99999 + %, Alfa Aesar) lumps and Fe (99.998%, Puratonic) powder in a molar ratio (Na,Li):Fe:As = 3:2:4 were placed into an alumina crucible, then kept inside a welded Nb container under ~0.8 bar of Ar atmosphere. The welded container was finally sealed in an evacuated quartz ampoule. The ampoule was heated directly up to 1050 °C, stayed at this temperature for 1 h, afterward slowly cooled down to 750 °C with a rate of 3 °C/h and then heater was turned off while the ampoule was still kept in the furnace. 2D plate-like-shaped single crystals with shiny *ab*-plane surfaces were mechanically detached from a flux and typical sizes were around ~440.3 mm³. Since the grown crystals were highly sensitive to air and moisture, each step of physical measurement preparations were also done in an Ar-filled glovebox. The crystalline phase was determined by the powder x-ray diffraction using Cu K_α radiation at room temperature. To avoid oxidation and compensate the preferred orientation of single crystals, a sealed quartz capillary was adopted with grounded as-grown crystals for powder diffraction measurements. To measure the (00*l*) reflection peak, a piece of single crystal with the shiny *ab*-plane surfaces was sandwiched between kapton tapes. Rietveld refinements of the diffraction pattern were performed using Fullprof program. In particular, inductively coupled plasma atomic photoemission spectroscopy (ICP-AES) was carried out on a piece of optimally doped Na_{0.95}Li_{0.05}FeAs to check the elemental composition of Na and Li; a molar ratio of Na and Li was found as Na: Li = 0.944: 0.056, which is close to the expected composition. Electrical resistivity was measured by the conventional four probe technique using a conductive silver epoxy in PPMS™ (Quantum Design). Magnetic susceptibility was measured with a vibrating sample magnetometer in PPMS™ and MPMS™ (Quantum Design).

It should be noted that SC transitions of all the samples were considerably broad as the estimated transition width ΔT extracted at temperatures of 10 and 90% of resistivity maximum was 7.5–15 K. Moreover, all the resistivity curves exhibited a temperature window of showing insulating behavior ($dp/dT < 0$) before the onset of SC transition similar to NaFe_{1-x}Cu_xAs system²³. In other doped Na 111 systems like NaFe_{1-x}Co_xAs²² and NaFe_{1-x}Rh_xAs²⁴, robust metallic behavior were observed in broad doping ranges. The former Cu doping was claimed to have isoelectronic doping while the latter two involving large electron doping was inevitably accompanied by large chemical potential shift. As Li does not bring additional charge carriers to the systems, the effect of disorder-induced electron localization on transport is likely pronounced to result in the insulating-like behaviors as in the case of NaFe_{1-x}Cu_xAs system.

Nuclear magnetic resonance. ⁷⁵As (nuclear spin $I = 3/2$) NMR was carried out in Na_{1-x}Li_xFeAs single crystals at an external field of 9.1 T and in the range of temperature 4.2–100 K. Due to the extreme sensitivity of the samples to air and moisture, all the samples were carefully sealed into quartz tubes filled with Ar gas. The sealed sample was reoriented using a goniometer for the accurate alignment along the external field. The ⁷⁵As NMR spectra were acquired by a standard spin-echo technique with a typical $\pi/2$ pulse length 2–3 μ s. The nuclear spin–lattice relaxation rate T_1^{-1} was obtained by fitting the recovery of the nuclear magnetization $M(t)$ after a saturating pulse to following fitting function,

$$1 - M(t)/M(\infty) = A[0.9 \exp(-6t/T_1) + 0.1 \exp(-t/T_1)]$$

where A is a fitting parameter. We also measured ²³Na NMR spectra for $x = 0.04$. As shown in Supplementary Fig. 6, we confirm that the ²³Na is barely influenced by the T_0 phase transition.

Data availability. The data that support the findings of this study are available from the corresponding authors (S.H.B. or K.H.K.).

Received: 28 November 2017 Accepted: 3 May 2018

Published online: 30 May 2018

References

- Fernandes, R. M., Chubukov, A. V. & Schmalian, J. What drives nematic order in iron-based superconductors? *Nat. Phys.* **10**, 97–104 (2014).
- Böhmer, A. E. & Meingast, C. Electronic nematic susceptibility of iron-based superconductors. *C. R. Phys.* **17**, 90 (2015).
- Si, Q., Yu, R. & Abrahams, E. High-temperature superconductivity in iron pnictides and chalcogenides. *Nat. Rev. Mater.* **1**, 16017 (2016).
- Kuo, H.-H., Chu, J.-H., Palmstrom, J. C., Kivelson, S. A. & Fisher, I. R. Ubiquitous signatures of nematic quantum criticality in optimally doped Fe-based superconductors. *Science* **352**, 958–962 (2016).
- Yamakawa, Y., Onari, S. & Kontani, H. Nematicity and magnetism in FeSe and other families of Fe-based superconductors. *Phys. Rev. X* **6**, 021032 (2016).
- Fernandes, R. M. & Chubukov, A. V. Low-energy microscopic models for iron-based superconductors: a review. *Rep. Prog. Phys.* **80**, 014503 (2017).
- Yi, M., Zhang, Y., Shen, Z.-X. & Lu, D. Role of the orbital degree of freedom in iron-based superconductors. *Quantum Mater.* **2**, 57 (2017).
- Böhmer, A. E. & Kreisel, A. Nematicity, magnetism and superconductivity in FeSe. *J. Phys. Condens. Matter* **30**, 023001 (2018).
- Chubukov, A. V., Fernandes, R. M. & Schmalian, J. Origin of nematic order in FeSe. *Phys. Rev. B* **91**, 201105 (2015).
- Fernandes, R. M., Böhmer, A. E., Meingast, C. & Schmalian, J. Scaling between magnetic and lattice fluctuations in iron pnictide superconductors. *Phys. Rev. Lett.* **111**, 137001 (2013).
- Lu, X. et al. Nematic spin correlations in the tetragonal state of uniaxial-strained BaFe_{2-x}Ni_xAs₂. *Science* **345**, 657–660 (2014).
- Kretzschmar, F. et al. Critical spin fluctuations and the origin of nematic order in Ba(Fe_{1-x}Co_x)₂As₂. *Nat. Phys.* **12**, 560 (2016).
- Baek, S.-H. et al. Orbital-driven nematicity in FeSe. *Nat. Mater.* **14**, 210–214 (2015).
- Böhmer, A. E. et al. Origin of the tetragonal-to-orthorhombic phase transition in FeSe: a combined thermodynamic and NMR study of nematicity. *Phys. Rev. Lett.* **114**, 027001 (2015).
- Baek, S.-H. et al. Nematicity and in-plane anisotropy of superconductivity in β -FeSe detected by ⁷⁷Se nuclear magnetic resonance. *Phys. Rev. B* **93**, 180502 (2016).
- Wang, X. C. et al. The superconductivity at 18 K in LiFeAs system. *Solid State Commun.* **148**, 538–540 (2008).
- Tapp, J. H. et al. LiFeAs: an intrinsic FeAs-based superconductor with $T_c = 18$ K. *Phys. Rev. B* **78**, 060505 (2008).
- Li, Z. et al. ⁷⁵As NQR and NMR studies of superconductivity and electron correlations in iron arsenide LiFeAs. *J. Phys. Soc. Jpn* **79**, 083702 (2010).
- Parker, D. R. et al. Structure, antiferromagnetism and superconductivity of the layered iron arsenide NaFeAs. *Chem. Commun.* **2009**, 2189–2191 (2009).
- Parker, D. R. et al. Control of the competition between a magnetic phase and a superconducting phase in cobalt-doped and nickel-doped NaFeAs using electron count. *Phys. Rev. Lett.* **104**, 057007 (2010).
- Chen, G. F., Hu, W. Z., Luo, J. L. & Wang, N. L. Multiple phase transitions in single-crystalline Na_{1- δ} FeAs. *Phys. Rev. Lett.* **102**, 227004 (2009).
- Wang, A. F. et al. Phase diagram and calorimetric properties of NaFe_{1-x}Co_xAs. *Phys. Rev. B* **85**, 224521 (2012).
- Wang, A. F. et al. Phase diagram and physical properties of NaFe_{1-x}Cu_xAs single crystals. *Phys. Rev. B* **88**, 094516 (2013).
- Steckel, F. et al. Crystal growth and electronic phase diagram of 4d doped Na_{1- δ} Fe_{1-x}Rh_xAs in comparison to 3d-doped Na_{1- δ} Fe_{1-x}Co_xAs. *Phys. Rev. B* **91**, 184516 (2015).
- Kitagawa, K., Mezaki, Y., Matsubayashi, K., Uwatoko, Y. & Takigawa, M. Crossover from commensurate to incommensurate antiferromagnetism in stoichiometric NaFeAs revealed by single-crystal ²³Na, ⁷⁵As-NMR experiments. *J. Phys. Soc. Jpn* **80**, 033705 (2011).
- Ma, L. et al. ²³Na and ⁷⁵As NMR study of antiferromagnetism and spin fluctuations in NaFeAs single crystals. *Phys. Rev. B* **83**, 132501 (2011).
- Ning, F. L. et al. Contrasting spin dynamics between underdoped and overdoped Ba(Fe_{1-x}Cox)₂As₂. *Phys. Rev. Lett.* **104**, 037001 (2010).
- Nakai, Y. et al. Normal-state spin dynamics in the iron-pnictide superconductors BaFe₂(As_{1-x}P_x)₂ and Ba(Fe_{1-x}Cox)₂As₂ probed with NMR measurements. *Phys. Rev. B* **87**, 174507 (2013).
- Takeda, H. et al. Substitution effects on the local magnetic properties of Ba(Fe_{1-x}Cu_x)₂As₂: a site-selective ⁷⁵As and ⁶³Cu NMR study. *Phys. Rev. Lett.* **113**, 117001 (2014).
- Lifshitz, I. M. Anomalies of electron characteristics of a metal in the high pressure region. *Sov. Phys. JETP* **11**, 1130 (1960).
- Nakai, Y. et al. Systematic ⁷⁵As NMR study of the dependence of low-lying excitations on F doping in the iron oxypnictide LaFeAsO_{1-x}F_x. *Phys. Rev. B* **79**, 212506 (2009).
- Ji, G. F. et al. Simultaneous optimization of spin fluctuations and superconductivity under pressure in an iron-based superconductor. *Phys. Rev. Lett.* **111**, (107004) (2013).
- Dioguardi, A. P. et al. Coexistence of cluster spin glass and superconductivity in Ba(Fe_{1-x}Cox)₂As₂ for 0.060 $\leq x \leq$ 0.071. *Phys. Rev. Lett.* **111**, 207201 (2013).
- Dioguardi, A. P. et al. NMR evidence for inhomogeneous glassy behavior driven by nematic fluctuations in iron arsenide superconductors. *Phys. Rev. B* **92**, 165116 (2015).
- Hunt, A. W., Singer, P. M., Thurber, K. R. & Imai, T. ⁶³Cu NQR measurement of stripe order parameter in La_{2-x}Sr_xCuO₄. *Phys. Rev. Lett.* **82**, 4300 (1999).
- Imai, T. et al. Revisiting ⁶³Cu NMR evidence for charge order in superconducting La_{1.885}Sr_{0.115}CuO₄. *Phys. Rev. B* **96**, 224508 (2017).
- Imai, T. & Lee, Y. S. ¹³⁹La and ⁶³Cu NMR investigation of charge order in La₂CuO_{4+y} ($T_c = 42$ K). *Phys. Rev. B* **97**, 104506 (2018).
- Imai, T., Ahilan, K., Ning, F. L., McQueen, T. M. & Cava, R. J. Why does undoped FeSe become a high-T_c superconductor under pressure? *Phys. Rev. Lett.* **102**, 177005 (2009).

39. Wright, J. D. et al. Gradual destruction of magnetism in the superconducting family $\text{NaFe}_{1-x}\text{Co}_x\text{As}$. *Phys. Rev. B* **85**, 054503 (2012).
40. Zhou, R., Xing, L. Y., Wang, X. C., Jin, C. Q. & Zheng, G.-q. Orbital order and spin nematicity in the tetragonal phase of the electron-doped iron pnictides $\text{NaFe}_{1-x}\text{Co}_x\text{As}$. *Phys. Rev. B* **93**, 060502 (2016).
41. Luetkens, H. et al. The electronic phase diagram of the $\text{LaO}_{1-x}\text{F}_x\text{FeAs}$ superconductor. *Nat. Mater.* **8**, 305 (2009).
42. Ma, L. et al. Phase separation, competition, and volume-fraction control in $\text{NaFe}_{1-x}\text{Co}_x\text{As}$. *Phys. Rev. B* **90**, 144502 (2014).
43. Fernandes, R. M., Chubukov, A. V., Knolle, J., Eremin, I. & Schmalian, J. Preemptive nematic order, pseudogap, and orbital order in the iron pnictides. *Phys. Rev. B* **85**, 024534 (2012).
44. Chubukov, A. V., Efremov, D. V. & Eremin, I. Magnetism, superconductivity, and pairing symmetry in iron-based superconductors. *Phys. Rev. B* **78**, 134512 (2008).
45. Kang, J. & Tešanović, Z. Theory of the valley-density wave and hidden order in iron pnictides. *Phys. Rev. B* **83**, 020505 (2011).
46. Classen, L., Xing, R.-Q., Khodas, M. & Chubukov, A. V. Interplay between magnetism, superconductivity, and orbital order in 5-pocket model for iron-based superconductors: Parquet Renormalization Group Study. *Phys. Rev. Lett.* **118**, 037001 (2017).

Acknowledgements

This work was financially supported by the National Creative Research Initiative (2010-0018300) and Global Collaborative Research Projects (2016K1A4A3914691) through Korea's NRF, which is funded by Ministry of Science, ICT and Future Planning (MSIP). The work at Germany has been supported by the Deutsche Forschungsgemeinschaft (Germany) via DFG Research Grants BA 4927/2-1. D.V.E. acknowledges VW-foundation for partial financial support.

Author contributions

K.H.K. and B.S.L. have proposed and initiated the project. W.H.N., B.S.L., D.B. have grown single crystals and characterized transport and structure properties. S.H.B.

performed NMR measurements and analyzed data; S.H.B., D.V.E., and K.H.K. participated in writing of the manuscript. All authors discussed the results and commented on the manuscript.

Additional information

Supplementary Information accompanies this paper at <https://doi.org/10.1038/s41467-018-04471-7>.

Competing interests: The authors declare no competing interests.

Reprints and permission information is available online at <http://npg.nature.com/reprintsandpermissions/>

Publisher's note: Springer Nature remains neutral with regard to jurisdictional claims in published maps and institutional affiliations.



Open Access This article is licensed under a Creative Commons Attribution 4.0 International License, which permits use, sharing, adaptation, distribution and reproduction in any medium or format, as long as you give appropriate credit to the original author(s) and the source, provide a link to the Creative Commons license, and indicate if changes were made. The images or other third party material in this article are included in the article's Creative Commons license, unless indicated otherwise in a credit line to the material. If material is not included in the article's Creative Commons license and your intended use is not permitted by statutory regulation or exceeds the permitted use, you will need to obtain permission directly from the copyright holder. To view a copy of this license, visit <http://creativecommons.org/licenses/by/4.0/>.

© The Author(s) 2018